

# ARTIFACTS IN MAGNETIC RESONANCE IMAGING FROM METALS

L.H. Bennett, P.S. Wang, M.J. Donahue

*National Institute of Standards and Technology, Gaithersburg, MD 20899, USA*

Metallic biomedical implants, such as aneurysm clips, endoprostheses, and internal orthopedic devices give rise to artifacts in the magnetic resonance image (MRI) of patients. Such artifacts impair the information contained in the image in precisely the region of most interest, namely near the metallic device. Ferromagnetic materials are contraindicated because of the hazards associated with their movement during the MRI procedure. In less-magnetic metals, it has been suggested that the extent of the artifact is related to the magnetic susceptibility of the metal, but no systematic data appear to be available. When the susceptibility is sufficiently small, an additional artifact due to electrical conductivity is observed. We present an initial systematic study of MRI artifacts produced by two low susceptibility metals, titanium (relative permeability  $\mu_r \approx 1.0002$ ) and copper ( $\mu_r \approx 0.99998$ ), including experimental, theoretical, and computer simulation results.

87.59.Pw, 75.20.En

The recent report [1] of a fatal outcome when an MRI was performed on the head of a patient having a ferromagnetic intracerebral aneurysm clip in place reemphasized the importance of the magnetic properties of clips or other surgical materials placed in the human body. Currently, most of the clips and many of the other implants are made of non-ferromagnetic materials. Even so, when a patient with a “nonmagnetic” metal in the body is subjected to an MRI, an artifact is produced which causes a drop-out of signal near the metallic surface. This is an unfortunate circumstance, making it impossible to investigate a treated aneurysm, as the signal is degraded in precisely the region of most interest to the surgeon.

The artifacts produced in MRI by material magnetic susceptibility have been widely studied. For example, Patton [2] provides an overview of MR imaging and artifacts, and Lüdeke et al. [3] give a particularly complete discussion of susceptibility related effects caused by (nonconducting) spheres and cylinders. A recent study [4] reports on the influence of small quantities of iron particles on MR images, and includes a comparison of the size of the artifact as a function of the particle mass. There has been less attention paid to MRI artifacts caused by eddy currents, but such effects have been observed [5,6].

In this paper we report on artifacts in proton MR imaging produced by nonferromagnetic metals in an aqueous medium, including both experimental and theoretical results. In addition to an effect from the material susceptibility, we also observed an artifact caused by eddy currents in the metal. For materials with extremely low susceptibility (e.g., copper), the eddy current effect is the dominant artifact. For materials with a slightly larger susceptibility (e.g., titanium), both susceptibility and eddy current artifacts can be observed. The importance of the object’s geometry on the extent of the susceptibility-induced artifact is also demonstrated. In particular, we show and explain how increasing the length of a Ti rod can *decrease* the MRI artifact (a similar effect was reported but not explained in [4]), and give rise to a bimodal free induction decay frequency response.

The NMR imaging facility consists of a Bruker MSL-400 system with micro-imaging accessories. The spectrometer has a superconducting magnet of 9.394 T which corresponds to a  $^1\text{H}$  resonant frequency of  $\approx 400$  MHz. A set of gradient coils generate field gradients of  $9.785 \times 10^{-2}$  T/m,  $3.549 \times 10^{-2}$  T/m, and  $1.175 \times 10^{-2}$  T/m along the  $x$  (reading),  $y$  (phase-encoding), and  $z$  (slicing) axes respectively. A 15 mm wide by 30 mm high RF-coil was used for detecting nuclear spin-echo signals of the aqueous protons, with a  $(\pi/2)\text{-}\tau\text{-}\pi\text{-}\tau\text{-}$ echo pulse sequence. More details on the experimental setup can be found elsewhere [7].

We report here on experiments with 2 mm diameter copper and titanium rods of various lengths, submerged in water inside a 9 mm inner diameter NMR tube. The applied field was shimmed initially for best response with the NMR tube and water alone. The shimming was left untouched for the rest of the experiments. Each rod was aligned with its long axis parallel to the static field (i.e., along the  $z$ -axis), and was held in place at the lower end with a teflon disk. The position of the lower end of each rod was the same, with the longer rods extending farther up the NMR tube. The magnetic resonance images were taken with the  $z$ -coordinate slice height in the center of the detection coil, about 7 mm from the rod’s lower end.

We imaged copper rods of lengths between 4 mm and 25 mm. The (diamagnetic) susceptibility  $\chi_v$  of the material was  $-2 \times 10^{-5}$  (SI), and the resistivity was  $17 \mu\Omega\cdot\text{mm}$ . The Fourier transform of the NMR free induction decay

consisted of a single peak, and the MRI was essentially independent of the bar length. A representative image for a 15 mm Cu rod is shown in Fig. 1a. The dark areas indicate the presence of water, so in the absence of any artifact, the image would show the cross section of the copper rod as a 2 mm white disk centered inside a 9 mm black annulus of water. The white area here is larger than the rod, and has in particular a notable 4-lobe asymmetry. The low susceptibility and high conductivity of the copper and this asymmetry led us to suspect the artifact was due to eddy currents in the copper.

To test this conjecture, we imaged titanium rods of various lengths. The susceptibility of the titanium was  $2 \times 10^{-4}$  (SI), and the resistivity was  $530 \mu\Omega\cdot\text{mm}$ . Compared to the copper, the titanium is paramagnetic with  $|\chi_v|$  10 times larger, and the resistivity is over 30 times greater. Fig. 1b shows the MRI of an 8 mm Ti rod, at a cross sectional height 1 mm below the top of the rod. Notice the circular susceptibility artifact (the white region is about 4.5 mm across, more than twice the diameter of the bar). Compare this to Fig. 1c, which represents a cross section near the center of a 13 mm Ti rod. The artifact has a (this time dark) circular component, but exhibits mainly a 4-lobe shape similar in size to that seen in the copper rod. We surmise that the symmetric susceptibility artifact is decreased because the slice is taken at a greater distance from the pole faces (i.e., the ends of the bar), and that the 4-lobe artifact due to eddy currents is present in both the 8 mm and the 13 mm Ti bar images, but is hidden in the former by the larger susceptibility artifact.

As discussed in the introduction, it is understood that material susceptibility will distort the field uniformity, and also that this can lead to a broadening of the free induction decay line width. We are apparently the first to report a splitting of the frequency response, as illustrated in Fig. 1d, which is the Fourier transform of the free induction decay signal for the two Ti rod experiments. Both graphs show two peaks, but the second peak is more pronounced for the 13 mm rod. This phenomenon is examined in greater detail below.

These experimental results give strong evidence that metal objects produce MRI artifacts of two distinct natures, one due to the material's susceptibility and the second due to its conductivity. To explain these results in more detail, we developed a simple model, implemented that model as a computer simulation, and then compared the simulation results with the experiments. This model explains the observed artifacts by field inhomogeneities alone. It has two components, the first handling material susceptibility effects and the second deals with eddy current effects. Alternately, these may be considered effects associated with the static field and the RF field, respectively.

The susceptibility effects are modeled by a pair of monopoles, one at each end of the cylindrical rod. For an applied static field of strength  $B_0$  oriented along the positive  $z$ -axis, the  $z$ -component of the resultant field at point  $(x, y, z)$  is

$$B_z^{\text{static}} = B_0 + \frac{B_0\chi_v R^2}{4} \left\{ \frac{z - z_t}{[x^2 + y^2 + (z - z_t)^2]^{3/2}} - \frac{z - z_b}{[x^2 + y^2 + (z - z_b)^2]^{3/2}} \right\}, \quad (1)$$

where  $\chi_v$  is the material susceptibility,  $R$  is the radius of the bar, and  $z_t$  and  $z_b$  are the  $z$ -coordinates of the top and the bottom of the bar, respectively. For non-ferromagnetic materials the relative contributions of the in-plane components  $B_x$  and  $B_y$  are small enough to be neglected.

For this initial study we used a simplified eddy current model. First, replace the finite rod with an infinite cylinder, and then notice that at the frequencies of our RF pulse (400 MHz) the skin depth  $\delta = (f\pi\mu\sigma)^{-1/2}$  for metals is in the micron range ( $\delta_{\text{Cu}} = 3.3 \mu\text{m}$ , and  $\delta_{\text{Ti}} = 18 \mu\text{m}$ ). The eddy currents set up a magnetic field that exactly opposes the applied RF field below about one skin depth. Since the skin depth is negligible compared to the diameter of the rod (2mm), our cylinder can be approximated by a cylinder that is uniformly magnetized directly equal but opposite to the applied RF pulse. For an applied pulse parallel to the  $y$ -axis with amplitude  $B_{\text{applied}}^{\text{RF}}$ , the resultant field at position  $(x, y)$  has amplitude components

$$B_x^{\text{RF}} \approx -2xyB_{\text{applied}}^{\text{RF}}R^2(x^2 + y^2)^{-2} \quad (2)$$

$$B_y^{\text{RF}} \approx B_{\text{applied}}^{\text{RF}} \left[ 1 + R^2(x^2 - y^2)(x^2 + y^2)^{-2} \right], \quad (3)$$

where  $R$  is again the radius of the bar. Note that unlike the equations for  $B^{\text{static}}$ ,  $B^{\text{RF}}$  does not exhibit circular symmetry.

The static components of the field affect slice and line selection. Field inhomogeneities can shift the effective position (i.e., as seen by the reconstruction) of protons, increasing the apparent density in some regions and decreasing it in others. This effect is evident in Fig. 1b, where the white artifact is a false indication of a decrease in the proton

density, and in Fig. 1c where there are regions near the bar that are even darker than the undisturbed regions near the edge of the NMR tube. (For a detailed discussion of this effect see [3].) Conversely,  $B^{\text{RF}}$  does not affect slice or line selection, but rather only changes the strength of the RF pulse seen by each proton. If the RF pulse is optimized to give maximal response in the absence of eddy current counter-fields, then this effect can only reduce the apparent density at any location. For a first approximation, we modeled the attenuation factor of the spin echo signal by  $\alpha = -\sin(1.5|B^{\text{RF}}|\pi/B_{\text{applied}}^{\text{RF}})$  for  $\pi < 1.5|B^{\text{RF}}|\pi/B_{\text{applied}}^{\text{RF}} < 2\pi$ , and 0 otherwise. For small deviations from  $B_{\text{applied}}^{\text{RF}}$  this is the in-plane component of the nuclear magnetization moment resulting from a  $1.5\pi$  RF pulse.

The forward portion of the computer implementation (simulation of the MR data) was accomplished by partitioning the experimental volume into 0.1 mm cubic voxels, adjusting the proton densities of each voxel according to  $B^{\text{RF}}$  and the corresponding attenuation factor, and then using (1) to determine line slice (raysum) selection. Once the data were completely generated, the inverse portion of the simulation—the image reconstruction—was accomplished using a Bracewell convolution filter [8].

Figs. 2a,b show the resulting simulations corresponding to the 15 mm Cu and the 13 mm Ti rod experiments. A simulation of the 8 mm Ti rod experiment was also performed but is not shown. The simulations are all in qualitative agreement with the experiments. Furthermore, by running the simulation with either the susceptibility term or the eddy current term, we have verified that the 4-lobe artifact is explained by eddy currents, and that the susceptibility artifact for an MR image taken in the middle of a rod will decrease with increasing rod lengths.

Let us now investigate the resonance splitting in the free induction decay observed in Fig. 1d. If we use (1), fix  $r = \sqrt{x^2 + y^2}$  and allow  $z$  to vary, we obtain line profiles of the field strength along lines parallel to the  $z$ -axis, as illustrated in Fig. 2c for a 13 mm Ti rod, where the applied field  $B_0$  has been subtracted off. The field values at  $z$  heights near the center of the bar and also above and below the bar do not vary very much with in-plane distance  $r$  from the bar. The middle plateau corresponds to a field value of  $\approx -15 \mu\text{T}$ , and the outside regions level off at  $\approx 5 \mu\text{T}$ . These correspond to resonance frequencies of  $\approx -640$  Hz and 210 Hz off the nominal resonant frequency of 400 MHz, not too different from the frequencies of the peaks seen in the experimental free induction decay frequency response curve of Fig. 1d. A more accurate simulation based on (1) (taking into account, for example, the appropriate radial weighting) produces the curves presented in Fig. 2d, and explains the relative size of the peaks as a function of the rod length.

We have shown, via both experiment and theory, that MRI artifacts from metallic objects have two distinct origins and manifestations. The first artifact source is inhomogeneity in the static field due to the material susceptibility, causing the MRI algorithm to mipmap the reconstruction region. When the material susceptibility is small, a second type of artifact becomes important. This artifact type is a result of eddy currents set up in conductors by the high frequency RF pulses, creating magnetic counter-fields which change the effective amplitude of the RF pulses across the imaging region, thereby modifying the spin-echo signal and affecting the image reconstruction.

The susceptibility induced artifact has been extensively studied by others, and it is well understood that the magnitude of this effect scales with the material susceptibility. The importance of the object's geometry has perhaps not been properly appreciated, however. We show, for example, that the artifact produced in the center of a paramagnetic cylindrical rod is actually reduced by making the rod longer. Similarly, it has been understood that the susceptibility induced inhomogeneity can broaden the free induction decay resonance peak. We have shown that the field inhomogeneity from a simple rod can actually create a bimodal resonance response, and that this effect will vary with the length of the rod.

From a design standpoint, since the susceptibility induced artifact can be reduced by minimizing the susceptibility of the metallic part, one might hope to manage the eddy current induced effect by reducing the object's electrical conductivity. Note, however, that the magnitude of this effect scales with the object's width minus the skin depth. The skin depth at 400 MHz of even a relatively poor (for a metal) conductor like Ti is only  $18 \mu\text{m}$ , so the impact of a metal's relative conductivity on the size of the artifact is minimal.

We thank H.J. Brown for assistance with measurements and D.E. Mathews for assistance with sample preparation.

- [1] R.P. Klucznik, D.A. Carrier, R. Pyka, and R.W. Haid, *Radiology* **187**, 855 (1993).
- [2] J.A. Patton, *RadioGraphics* **14**, 1083 (1994).
- [3] K.M. Lüdeke, P. Röschmann, and R. Tischler, *Mag Res Imag* **3**, 329 (1985).
- [4] A. Alanen, S. Bondestam, and M. Komu, *Acta Radiologica* **36**, 92 (1995).
- [5] J.A. Malko, J.C. Hoffman Jr, and P.J. Jarrett, *Radiology* **173**, 563 (1989).
- [6] C.R. Camacho, D.B. Plewes, and R.M. Henkelman, *J Magn Reson Imaging (BEO)* **5**, 75 (1995).
- [7] P.S. Wang, S.G. Malghan, S.J. Dapkunas, K.F. Hens, and R. Raman, *J Mat Sci* **30**, 1059 (1995); *ibid* **30**, 1069 (1995); P.S. Wang, submitted to *J Mat Res* (1995).
- [8] R.N. Bracewell and A.C. Riddle, *Astrophysics J* **150**, 427 (1967).

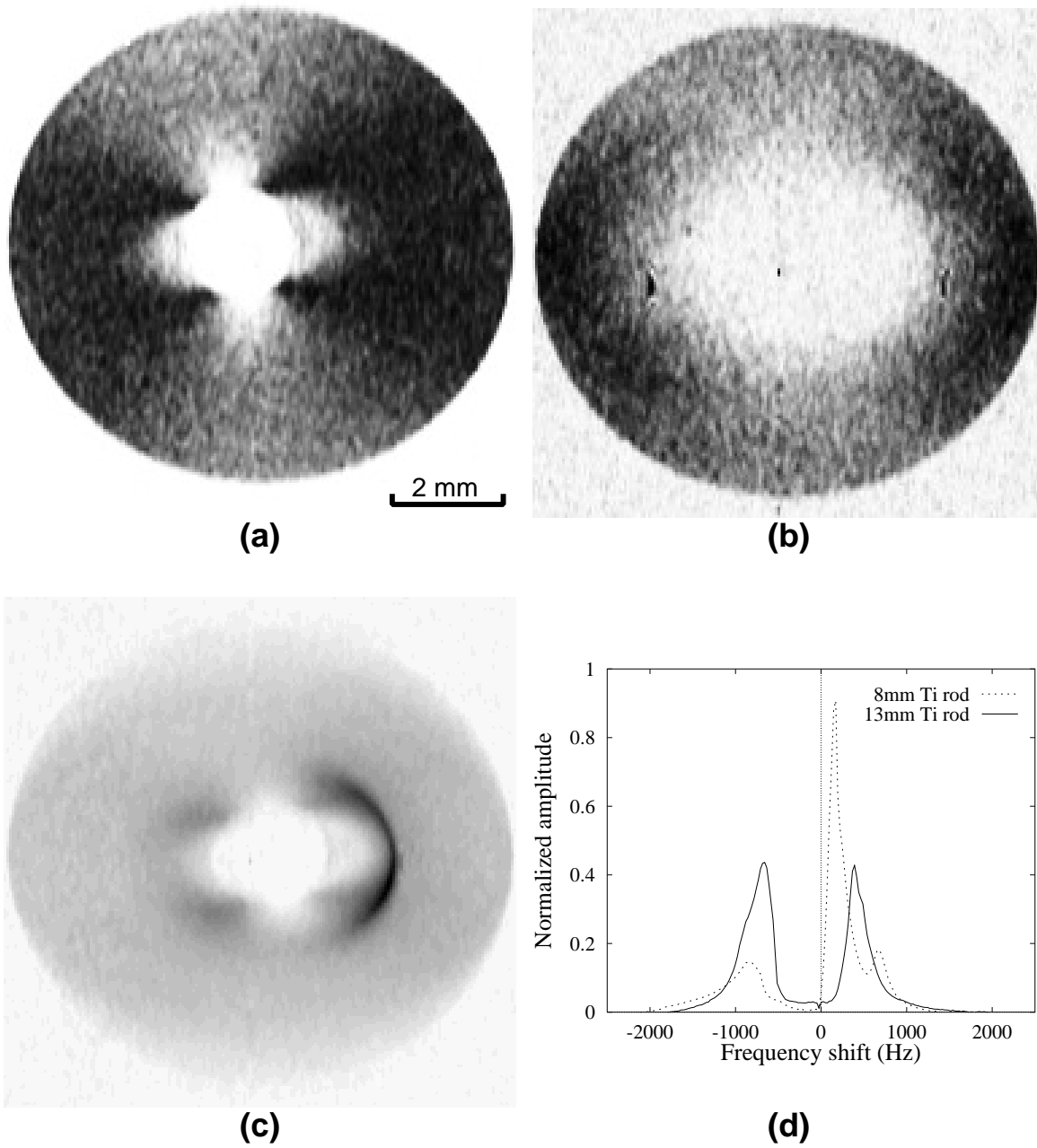


Fig. 1: Experimental results: (a) MR image cross section of a 15 mm Cu rod, (b) a 8 mm Ti rod, and (c) a 13 mm Ti rod; (d) Fourier transform of free induction decay for the 8 mm and the 13 mm Ti rods.

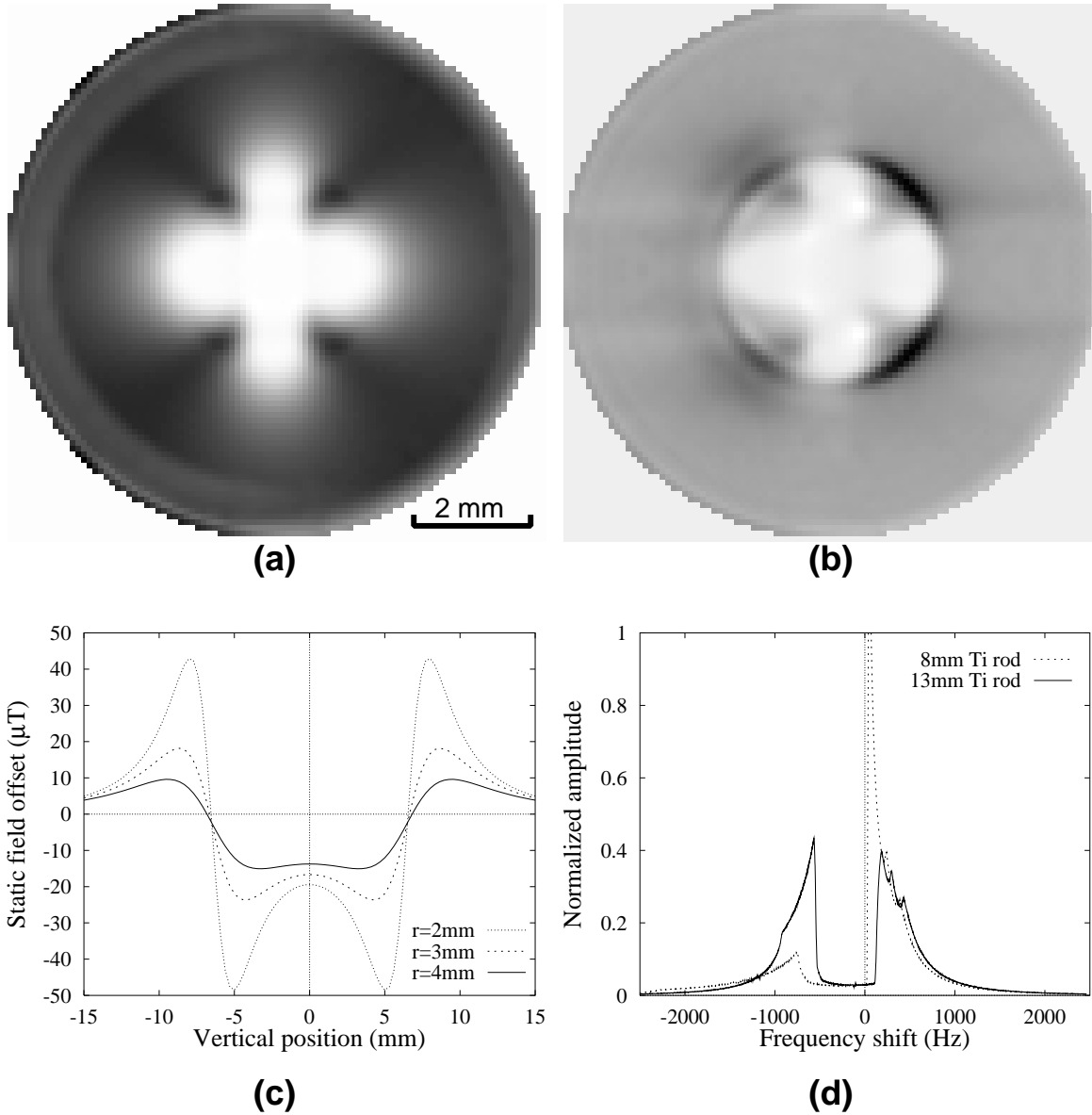


Fig. 2: Theoretical results: (a) Simulated MR image cross section of a 15 mm Cu rod, and (b) a 13 mm Ti rod; (c) Field strength  $B^{\text{static}}$  for 13 mm Ti rod along lines parallel to the  $z$ -axis at radial distances  $r = 2$  mm, 3 mm, and 4 mm; (d) Simulated Fourier transform of free induction decay for 8 mm and 13 mm Ti rods.